RRPA89050244 (25.P)

行政院國家科學委員會專題研究計畫成果報告

超晶格電子與原子結構研究

計畫類別：個別型計畫

計畫編號：NSC 89-2112-M-032-008

執行期間：88/08/01-89/10/31

個別型計畫：計畫主持人：彭維鋒
共同主持人：

整合型計畫：總計畫主持人：
子計畫主持人：

處理方法：☑可立即對外提供參考
□一年後可對外提供參考
□兩年後可對外提供參考

執行單位：淡江大學物理學系

中華民國九十年二月十四日

Charge transfer and hybridization effects in Ni_3Al and Ni_3Ga studies by x-ray-absorption spectroscopy and theoretical calculations

Y. K. Chang, K. P. Lin, and W. F. Pong[a)]
Department of Physics, Tamkang University, Tamsui 251, Taiwan

M.-H. Tsai
Department of Physics, National Sun Yat-Sen University, Kaohsiung 804, Taiwan

H. H. Hseih, J. Y. Pieh,[b)] and P. K. Tseng
Department of Physics, Tamkang University, Tamsui 251, Taiwan

J. F. Lee
Synchrotron Radiation Research Center, Hsinchu Science-based Industrial Park 300, Taiwan

L. S. Hsu
Department of Physics, National Chang-Hua University of Education, Chang-Hua 500, Taiwan

(Received 10 May 1999; accepted for publication 21 October 1999)

This work investigates the charge transfer and Al(Ga) p-Ni d hybridization effects in the intermetallic Ni_3Al (Ni_3Ga) alloy using the Ni $L_{3,2}$ and K edge and Al (Ga) K x-ray absorption near edge structure (XANES) measurements. We find that the intensity of near-edge features at the Ni L_3 edge in the Ni_3Al (Ni_3Ga) alloy decreased with respect to that of pure Ni, which implies a reduction of the number of unoccupied Ni $3d$ states and an enhancement of the Ni $3d$ state filling in the Ni_3Al (Ni_3Ga) alloy. Two clear features are also observed in the Ni_3Al (Ni_3Ga) XANES spectrum at the Al (Ga) K edge, which can be assigned to unoccupied Al $3p$-(Ga $4p$-) derived states in Ni_3Al (Ni_3Ga). The threshold at the Al K-edge XANES for Ni_3Al shifts towards the higher photon energy relative to that of pure Al, suggesting that Al loses some p-orbital charge upon forming Ni_3Al. On the other hand, the Ni K edge shifts towards the lower photon energy in Ni_3Al (Ni_3Ga) relative to that of pure Ni, suggesting a gain of charge at the Ni site. Thus both Al and Ni K-edge XANES results imply a transfer of charge from Al $3p$ orbital to Ni sites. Our theoretical calculations using the spin-polarized first-principles pseudofunction method agree with these results. © *2000 American Institute of Physics.* [S0021-8979(00)03603-3]

I. INTRODUCTION

The intermetallic Ni_3Al compound has received extensive attention owing to its potential applications in high-temperature structural materials.[1] The unique properties of the Ni_3Al compound are principally attributed to the nature of its electronic and atomic structures. It is well known that the atomic structure of Ni_3Al has a cubic $L1_2$-type order. In this structure Al occupies the cubic corners and Ni occupies the face centers so that each Ni atom is coordinated with 8 Ni and 4 Al atoms in the first shell. Extended electron energy-loss fine structure studies were performed on the local atomic structure of Ni_3Al.[2] On the other hand, Muller *et al.*[3] performed Ni $L_{3,2}$-edge electron energy loss spectroscopy (EELS) to investigate the electronic structure of segregated grain boundaries in Ni_3Al with and without boron dopants. This study indicated that boron tends to increase the cohesive strength, possibly due to the enhancement of boron-induced ductility in Ni_3Al. Owing to the absence of a core level shift in the Ni L_3-edge EELS spectra of Ni_3Al from that of pure Ni, Muller *et al.* concluded that little net charge is transferred between Al and Ni sites in Ni_3Al. And Auger electron[4] and x-ray photoemission[5] measurements suggested that charge transfer only influences slightly the filling of the Ni $3d$ band in Ni_3Al. Iotova *et al.* systematically calculated electronic structures and elastic properties for the Ni_3X (X=Mn, Al, Ga, Ge, and Si) series and found an increasing trend of shear module that goes from Ni_3Mn to Ni_3Si.[6] This trend could be related to the anisotropic bonding charge density resulted from a combination of the charge transfer from X to Ni and a strong X p-Ni d (Mn d-Ni d in Ni_3Mn) hybridization effects in Ni_3X. Charge transfer and strong hybridization effects in Ni_3Al were also supported by previous electronic structure calculations.[7,8] Thus, there were discrepancies between theoretical results and the interpretations of EELS, Auger, and x-ray photoemission data. As generally known, the charge transfer between X and Ni sites and the density of X p-Ni d hybridized states above the Fermi level in the Ni_3X systems should be observable for all excitations involving outermost X p or Ni d final states from x-ray absorption near edge structure (XANES) spectra. Here, we focus on the understanding of the p-d hybridization between Al and Ni in Ni_3Al and between Ga and Ni in Ni_3Ga and clarification of the controversy over the charge transfer between Al (Ga) and Ni sites in Ni_3Al (Ni_3Ga). How charge transfer influences the filling of the Ni $3d$ band in Ni_3Al (Ni_3Ga) will be addressed.

a)Electronic mail: wfpong@mail.tku.edu.tw
b)Author to whom correspondence should be addressed; present address: China Textile Institute, Tu-Chen, Taiwan.

 © 2000 American Institute of Physics

TABLE I. The parameters of the lattice constant (a_0), muffin-tin radii (R_{mt}), and number of plane waves which we used to expand the psuedofunction (PSF), charge density ρ, and potential V at the interstitial and nonspherical regions.

	a_0(a.u.)	$R_{mt(a.u.)}$	PSFs	ρ	V
Ni	6.6519[a]	2.17	13^3	25^3	25^3
Ni_3Al	6.7378	2.35 (Ni)	9^3	17^3	17^3
		2.38 (Al)			
Ni_3Ga	6.7841	2.35 (Ni)	9^3	17^3	17^3
		2.44 (Ga)			
Al	7.6535[a]	2.30	11^3	21^3	21^3

[a]C. Kittel, *Introduction to Solid State Physics*, 7th ed. (J Wiley, New York, 1996).

The chemical shifts of the absorption edge in the XANES spectra are strongly related to the charge transfer between Al (Ga) and Ni sites. We also analyzes the electronic structures of Ni_3Al (Ni_3Ga) obtained by combining Ni $L_{3,2}$- and K edge and Al (Ga) K-edge XANES measurements and the spin-polarized first-principles electronic structure calculations using the pseudofunction method.

II. EXPERIMENT

The XANES measurements were performed using the high-energy spherical grating monochromator (HSGM) with an electron beam energy of 1.5 GeV and a maximum stored current of 200 mA at the Synchrotron Radiation Research Center (SRRC), Hsinchu, Taiwan. The spectra of the Ni $L_{3,2}$ edge and Al K-edge XANES were measured using the sample drain current mode at the room temperature. The Ni and Ga K-edge XANES measurements were also performed in a total electron mode at the wiggler beamline of SRRC. A Si(111) double crystal monochromator was used to record the spectra. The typical resolution of the spectra was 0.4–0.5 eV for HSGM and ~2 eV for wiggler beamlines. The samples were prepared by arc melting after argon backfill, as described in elsewhere.[9] The single phase and concentration of the samples were confirmed using x-ray diffraction and energy-dispersive x-ray fluorescence analysis.

III. THEORY

The spin-polarized first-principles pseudofunction (PSF) method[10] was employed to calculate the projected density-of-states (DOS) and the amount of electron charge occupying each valence state at the Ni and Al sites in the Ni_3Al and Ni_3Ga alloys and pure Ni and Al reference samples. In this method, the potential was divided into spherical potentials within the muffin-tin spheres and a plane-wave expanded potential that extends throughout the crystal, which includes interstitial potential and the nonspherical part of potentials within muffin-tin spheres. PSFs are smooth mathematical functions constructed by continuously and differentially extending the muffin-tin-orbital tails into muffin-tin spheres. They are simply devised to calculate the interstitial and nonspherical parts of matrix elements efficiently[10] through plane waves using the fast Fourier transform technique. Table I lists the lattice constant (a_0), muffin-tin radii (R_{mt}), and number of plane waves used to expand the PSF, nonspherical and interstitial charge density ρ and potential V for all the samples. The lattice constants of Ni_3Al and Ni_3Ga were determined according to the x-ray diffraction measurements. The unit-cell parameters and atomic positions were deduced from x-ray crystallograph table.[11] Muffin-tin radii chosen for Ni, Al, and Ga are roughly proportional to their covalent radii[12] with the constraint that all muffin-tin spheres do not overlap. We have chosen the cubic unit cell for Ni_3Al, Ni_3Ga, and pure Ni and Al metals, although they have a face-centered-cubic (fcc) base structure. For pure Ni and Al, there are four Ni or Al atoms per unit cell. For Ni_3Al and Ni_3Ga, there are three Ni atoms and one Al or Ga atom in the unit cell. In this study, four special **k** points of Chadi and Cohen for a simple cubic lattice were used to obtain the self-consistent charge density and potential.[13] To obtain partial DOSs, we have chosen the Monkhorst–Pack special **k** points with $\mathbf{q}=4$.[14] Totally, twenty special **k** points were sampled to obtain partial DOSs.

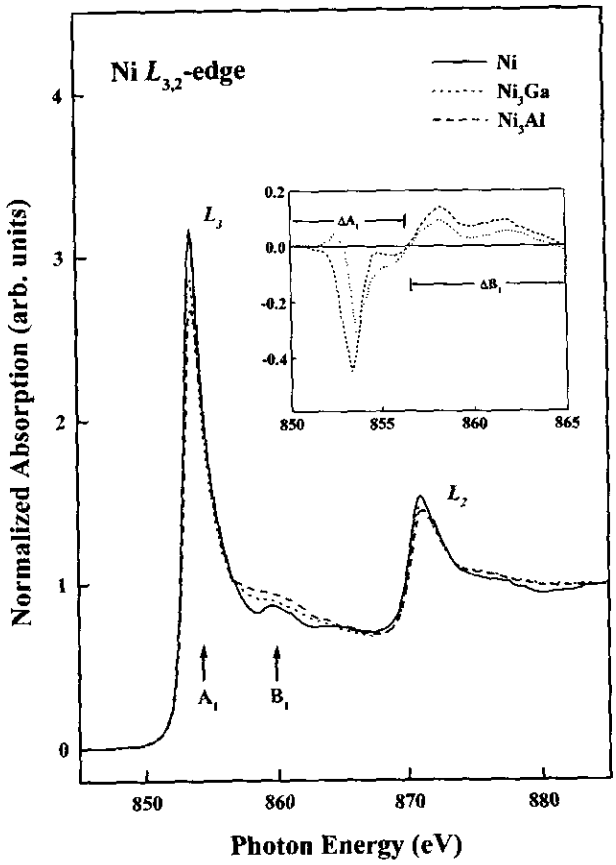

FIG. 1. Normalized Ni $L_{3,2}$-edge x-ray absorption spectra of Ni_3Al and Ni_3Ga alloys and pure Ni metal at room temperature. The inset shows the Ni L_3-edge difference curve for Ni_3Al and Ni_3Ga with respect to pure Ni.

IV. RESULTS AND DISCUSSION

Figures 1 and 2 display the Ni $L_{3,2}$ and Al K-edge XANES spectra of the Ni_3Al and Ni_3Ga alloys, respectively, in which pure Ni and Al metals are regarded as references. All of the spectra shown in these figures were divided by the incident intensity I_0 and then normalized to an edge jump of unity. The normalization procedure was implemented by matching the absorption coefficients from the pre-edge re-

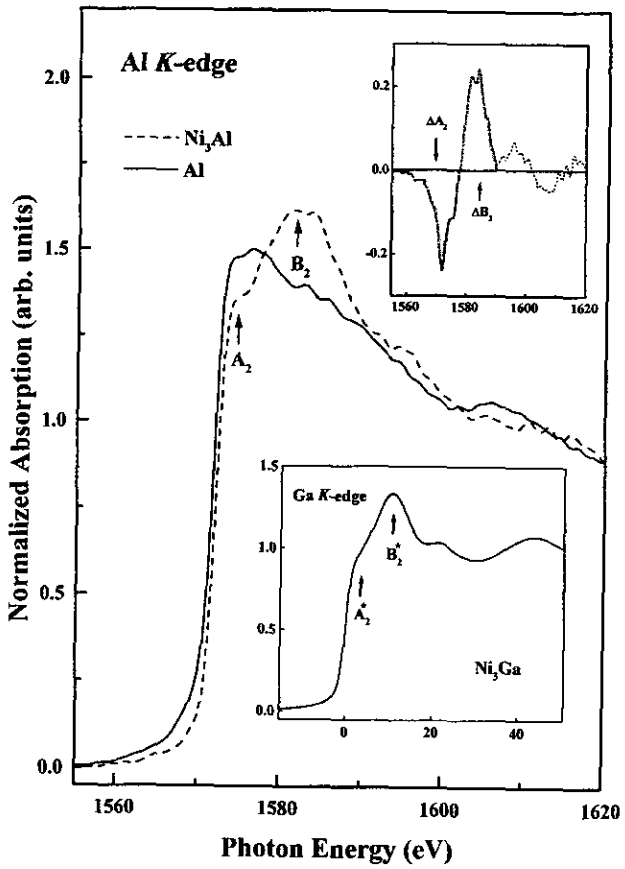

FIG. 2. Normalized Al K-edge x-ray absorption spectra of Ni_3Al (dot line) and pure Al (solid line) at room temperature. The lower inset shows the normalized Ga K-edge x-ray absorption spectra of the Ni_3Ga alloy, in which the zero energy was selected at the reflection point of the edge. The upper inset shows the Al K-edge difference curve between Ni_3Al and Al. The area under the difference curve in the region of interest is darkened.

gion at L_3 edge to 20 eV above the L_2 edge of Ni and keep the same area in the energy range between 1660 and 1670 eV (not fully shown in Fig. 2) as that of the Al K edge. By using the dipole-transition selection rules, we can assign the white line features at the Ni $L_{3,2}$-edge (labeled L_3 and L_2) XANES to the transitions from the Ni $2p_{3/2}$ and $2p_{1/2}$ ground states to the unoccupied Ni $3d$ final states. The general spectral lineshapes in the Ni $L_{3,2}$-edge XANES spectra of Ni_3Al and Ni_3Ga display similar white-line features (labeled as A_1) above the Ni L_3 edge. However, their intensities are reduced considerably in comparison with those of pure Ni. The dependence of the general behavior of the spectra's line shape and intensity on the photon energy for Ni_3Al and Ni_3Ga are similar except that the intensity of the white-line features A_1 (the higher energy satellite structure, B_1) at the Ni L_3 edge is slightly lower (larger) in the Ni_3Al spectrum than in the Ni_3Ga spectrum. The difference curve (hereinafter referred to as ΔA_1 and ΔB_1) of the Ni L_3-edge XANES in Ni_3Al and Ni_3Ga with respect to pure Ni are shown in the inset of Fig. 1. No significant energy shifts of the highest peak in the Ni $L_{3,2}$-edge XANES spectra from that of pure Ni are observed for both alloys. Our data are in agreement with earlier Ni $L_{3,2}$-edge EELS measurements made on the $Ni_{1-x}Al_x$ alloys.[3] In addition, the satellite structures B_1 for both Ni_3Al and Ni_3Ga are enhanced and broadened relative to that of pure Ni. This satellite structure can be assigned to the excitation of electrons from Ni $2p_{3/2}$ to Ni $4s$ states.[15] Our results indicate a decrease in the intensity of white-line features A_1 at the Ni L_3 edge for both Ni_3Al and Ni_3Ga alloys relative to that of pure Ni, which corresponds to a decrease of the number of unoccupied Ni $3d$ states and an enhancement of the Ni $3d$-state filling.

Figure 2 displays the Al K-edge XANES spectra for Ni_3Al and pure Al. In the Ni_3Al spectrum, the intensity of feature A_2, which is located between ~1573 and 1577 eV, is markedly reduced and the reflection point of the threshold clearly shifts towards the higher energy with respect to that of pure Al. In addition, a prominent feature B_2 (located between ~1577 and 1590 eV) is significantly enhanced in the Ni_3Al spectrum. The lower inset of this same figure reveals a similar behavior of features A_2^* and B_2^* at the Ga K-edge XANES in the Ni_3Ga spectrum (There was a difficulty in comparing the Ga K-edge XANES spectrum with that of pure Ga because pure Ga has a low melting point and different bonding properties at room temperature). According to the dipole-transition selection rules, the features A_2 (A_2^*) and B_2 (B_2^*) in the Al (Ga) K-edge XANES spectra as shown in the (inset) of Fig. 2 can be assigned to the transitions to unoccupied Al $3p$-(Ga $4p$-) derived states, which hybridize with the Ni $3d/4sp$ states. As mentioned earlier, the inflection point in the Ni_3Al XANES spectrum at the Al K edge apparently shifts towards the higher photon energy than those of pure Al. This suggests that Al loses some p-orbital charge upon forming Ni_3Al because the loss of some $3p$ electrons reduces the screening of the Al nuclear charge and consequently lowers the $1s$ core level energy of Al. We also determine the difference of the densities of Al $3p$-derived states for Ni_3Al and pure Al just above the Fermi level. A comparison is made of the areas under the Al K-edge XANES spectra as shown in Fig. 2. The edge energy E_0 in the Ni_3Al spectra is aligned with that of pure Al. We assume that the dipole transition matrix element at the Al K edge is the same for both Ni_3Al and pure Al. We also adopt the findings of Tamura *et al.* for pure Al that its unoccupied p states spread up to ~30 eV above the Fermi level[16] and that the area under the difference curve (hereinafter denoted as ΔA_2 and ΔB_2) as shown in the upper inset of Fig. 2 is proportional to the difference in the densities of unoccupied Al $3p$-derived states between Ni_3Al and pure Al. The ranges of integration are from 1555.0 to 1577.5 eV and from 1577.5 to 1590.0 eV, respectively, for ΔA_2 and ΔB_2. The integration for $\Delta A_2+\Delta B_2$ yields 0.17 (-1.56 ± 0.08 and 1.73 ±0.09, respectively, for ΔA_2 and ΔB_2). Thus, the number of unoccupied Al $3p$-derived states increases in Ni_3Al relative to that of pure Al. In other words, Al loses some p-orbital charge in consistent with that suggested by the shift of the threshold of the spectrum.

Ni $L_{3,2}$- and Al K-edge XANES results suggest a charge transfer from the Al $3p$ orbitals to Ni sites. However, in metals the charge count at the atomic site (Wigner Seitz volume) tends to remain neutral, i.e., only a small amount of net charge transfer possibly occurs upon alloying. This property is due to the itinerant nature of conduction electrons which automatically adjust their distribution to minimize the elec-

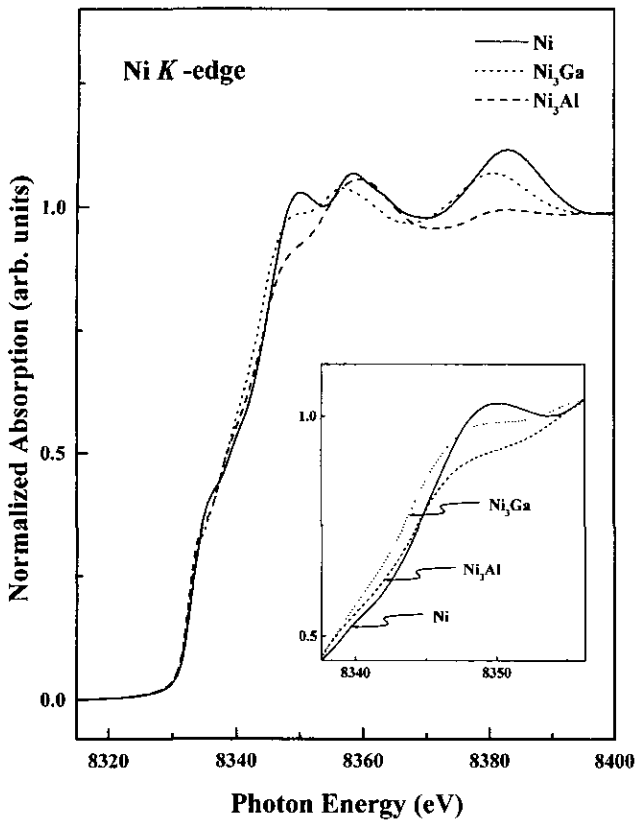

FIG. 3. Normalized Ni K-edge x-ray absorption spectra of the Ni_3Al and Ni_3Ga alloys and pure Ni at room temperature. The region of threshold edge in the inset is on a magnified scale.

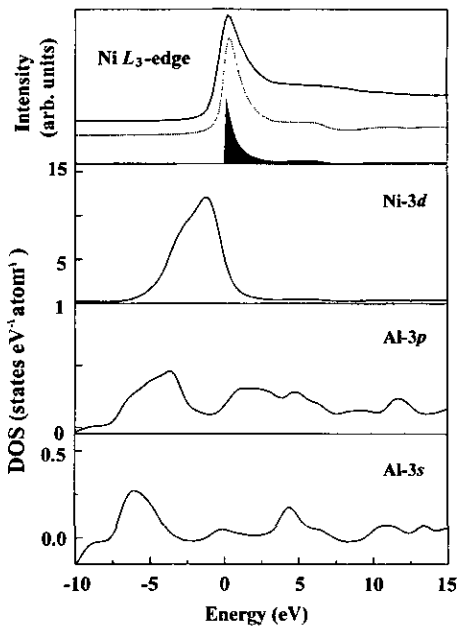

FIG. 4. Comparison of the Ni L_3-edge x-ray absorption near edge features (upper solid-line) with a convolution of the theoretical Ni d-projected DOS with core-hole lifetime and instrumental broadening (upper dashed-line) for Ni_3Al. The spectra have been aligned at the position of the first peak, and the intensity units have been normalized arbitrarily. The darkened area is the theoretical Ni d-projected DOS above the Fermi level, which is defined as the zero energy.

trostatic energy. Although electroneutrality is the general rule, charge redistribution of localized d electrons and itinerant sp type conduction electrons according to the relative electronegativity of the constituent metal atoms can still occur without any significant net charge flow on and off a site in alloys.[17–19] One would intuitively expect that the Ni levels should shift to the lower photon energy in Ni_3Al opposite to the shift to the higher photon energy of the Al p-derived states. However, the Ni $3d$ states in Ni_3Al and Ni_3Ga do not shift noticeably towards the lower photon energy at the Ni $L_{3,2}$ edge as shown in Fig. 1. Thus, we argue that the charge transfer occurs not only through the Al $3p$(Ga $4p$)-Ni $3d$ hybridized states, but also through the rehybidized s-p-d states involving one or two sites in Ni_3Al (Ni_3Ga). The involvement of conduction electrons of Ni p character in rehybridization can be evidenced in the Ni K-edge XANES, which probes the unoccupied Ni $4p$-derived states above the Fermi level. Figure 3 displays the Ni K-edge XANES of Ni_3Al, Ni_3Ga, and pure Ni. According to this figure, the absorption intensity above the main edge decreases noticeably and the shift of their main edges towards the lower photon energy for both Ni_3Al and Ni_3Ga are comparable with that of pure Ni. The pre-edge shoulder in the Ni K-edge XANES can be attributed to the Ni $1s$ to $3d$ transition through the Ni p-d rehybridization.[18] A reduction of the Ni K near edge intensity corresponds to the reduction of the number of unoccupied Ni $4p$-derived states, which implies an enhancement of the number of occupied Ni $4p$-derived states and a gain of Ni $4p$-orbital charge upon alloying. To maintain local charge neutrality, Ni must lose some s-orbital charges in both Ni_3Al and Ni_3Ga and the density of unoccupied Ni s-derived states in the vicinity of the Fermi level should increase in both Ni_3Al and Ni_3Ga relative to that of pure Ni. This indeed can be found in the satellite structure B_1 at the Ni L_3 edge of the XANES spectra for Ni_3Al and Ni_3Ga as shown in Fig. 1, which can be seen to be relatively dispersive and stronger. This observation is consistent with the difference curve of the Ni L_3-edge spectra between the alloys and pure Ni as shown in the inset of Fig. 1. The intensities of ΔA_1 (between 850.0 and 856.6 eV) and ΔB_1 (between 856.6 and 865.0 eV) were integrated separately for the Ni_3Al and Ni_3Ga spectra. The integration yielded -0.62 ± 0.03 and 0.60 ± 0.03 for Ni_3Al and -0.38 ± 0.02 and 0.33 ± 0.02 for Ni_3Ga for ΔA_1 and ΔB_1, respectively. These results indicate that the loss in ΔA_1 (indicating that Ni $3d$ orbitals gain electron charge) is almost compensated by the gain of ΔB_1 (indicating that Ni $4s$ orbital loses electron charge) in Ni_3Al and Ni_3Ga.

Figures 4 and 5 compare Ni L_3-and Al K-edge XANES spectra with calculated Ni d-projected and Al p-projected DOS of Ni_3Al, respectively. The darkened area shows the theoretical Ni d-projected and Al p-projected DOS above the Fermi level. The upper solid curve is the Ni L_3- and Al K-edge absorption spectra at the region of XANES. The dashed curve in the middle represents the theoretical Ni d-projected (Al p-projected) DOS broadened with a Lorentzian of 0.3 eV (0.42 eV) to simulate the core-hole lifetime[20] and convoluted with a Gaussian function of 0.4 eV (0.5 eV) to simulate the experimental resolution. According to Figs. 4 and 5, the Ni $3d$ states lie predominantly below and near the Fermi level with a relatively small DOS above the threshold region in comparison with those of Ni $4sp$ and Al $3sp$ states.

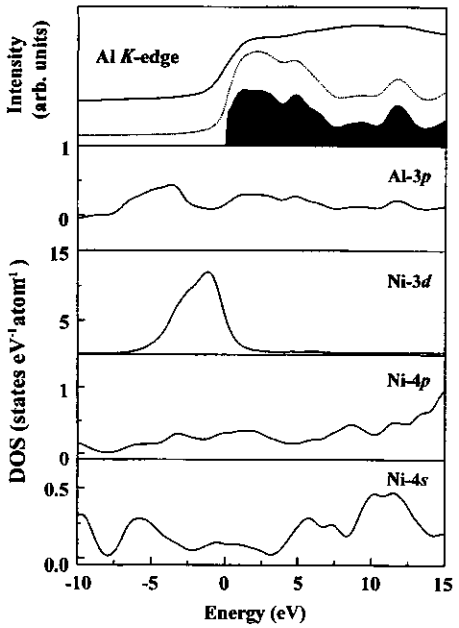

FIG. 5. Comparison of the Al *K*-edge x-ray absorption near edge features (upper solid-line) with a convolution of the theoretical Al *p*-projected DOS with core-hole lifetime and instrumental broadening (upper dashed-line) for Ni_3Al. The spectra have been aligned at the position of the first peak and the intensity units have been normalized arbitrarily. The darkened area is the theoretical Al *p*-projected DOS above the Fermi level, which is defined as the zero energy.

The DOSs for Ni $4sp$ and Al $3sp$ states spread over a wide energy range because they are more delocalized or extended. Our calculations also reveal that the white-line features A_1 and the satellite structure B_1 observed at Ni L_3-edge XANES in Fig. 1 is primarily contributed by Ni $3d$-derived states, which hybridize with the Al $3sp$ states. On the other hand, peaks A_2 and B_2 at the Al *K*-edge XANES of Ni_3Al shown in Fig. 5 can be attributed to the Al $3p$-derived states, which hybridize with the Ni $3d/4sp$ states. In particular, the Al $3p$-Ni $3d/4sp$ hybridized states are found to contribute significantly to features B_2 at the Al *K*-edge XANES spectra of Ni_3Al. Similar results have also been obtained for the Ni_3Ga alloy. These results agree with our experimental data and confirm the presence of strong Ni–X hybridized bonds in the Ni-based intermetallic Ni_3X systems.[4–8]

Table II summarizes the calculated numbers of electrons (e) occupying the valence orbitals of Ni and Al in the alloy and pure Ni and Al. Although recent augmented plane wave (APW) calculations showed that there is no unique definition of charge at a particular atomic site and charge transfer between two sites and they were found to depend on the muffin-tin radii of Al and Ni,[21,22] we believe these problems are characteristics of the plane-wave based methods because these methods cannot unambiguously assign interstitial charge to any particular atom. In contrast, the PSF method used in this study has an atom-centered muffin-tin-orbital basis set. Charges and charge transfer can be unambiguously determined through the occupation numbers of muffin-tin orbitals. Table II shows that Ni $3d$ states in Ni_3Al and Ni_3Ga gain a significant amount of charge relative to that of pure Ni, which qualitatively explain the variation of white-line features A_1 between alloys and pure Ni at the Ni L_3 edge as shown in Fig. 1. Since the intensity of A_1 is proportional to the density of unoccupied Ni $3d$ states, these calculated results imply a decrease of A_1 intensities in Ni_3Al and Ni_3Ga relative to that of pure Ni. Results of Ni d electron counts in Ni_3Al and pure Ni shown in Table II are consistent with earlier calculations.[7] The slightly larger charge transfer from Al to Ni d orbitals in $Ni_3Al(0.29e)$ than that from Ga to Ni d orbitals in $Ni_3Ga(0.24e)$ agrees with the results of Ni L_3-edge measurements. These measurements reveal a slightly smaller intensity of Al in Ni_3Al than in Ni_3Ga. The calculated number of Al p electrons decreases slightly from pure Al (1.48e) to the alloy $Ni_3Al(1.46e)$, which corresponds to the results of Al *K*-edge XANES shown in Fig. 2. The calculated number of Al s electrons decreases from pure $Al(1.51e)$ to the Ni_3Al alloy $(1.20e)$. The calculated number of Ni s electrons decreases slightly from pure $Ni(0.58e)$ to $Ni_3Al/Ni_3Ga(0.54e)$. The numbers of s electrons transferred away from the Ni $4s$ orbital in the alloys are relatively small $(0.04e)$ comparing to that inferred from our experimental observations of a stronger B_1 features in Ni_3Al and Ni_3Ga than in pure Ni. These results agree with the earlier discussion that Ni d orbitals in the alloys gain some electron charges with the expense of non-d conduction electrons (s electrons). The direction of charge transfer is in accordance with the higher electronegativity for Ni (1.91) than for Al (1.61) and Ga (1.81). If $\Delta n(\mathrm{Ni})[\Delta n(\mathrm{Al})]$ is the difference in the electron counts in the Ni (Al) orbitals between Ni_3Al and pure Ni (Al), then $\Delta n(\mathrm{Ni}) = n_{\mathrm{spd}}(\mathrm{Ni_3Al}) - n_{\mathrm{spd}}(\mathrm{Ni})[\Delta n(\mathrm{Al}) = n_{\mathrm{sp}}(\mathrm{Ni_3Al}) - n_{\mathrm{sp}}(\mathrm{Al})]$. Δn's can be obtained from the numbers of electrons occupying Ni and Al orbitals given in Table II. The charge transferred into the Ni orbitals is $+0.26e$, which roughly equals the charge transferred away from the Al orbitals $(-0.33e)$ in the Ni_3Al alloy. This is consistent with the observation that the intensities of the white-line A_1 features are considerably reduced in Ni_3Al and Ni_3Ga as shown in Fig. 1, which implies a gain of Ni $3d$-orbital charge. The Ni $L_{3,2}$-edge XANES spectra do not have any noticeable shifts relative to that of pure Ni, suggesting some non-d charge depletion at the Ni sites in the alloy. Moreover, the absorption intensity above the Ni *K*-edge XANES in Ni_3Al and Ni_3Ga decreases relative to that of pure Ni as shown in Fig. 3, which suggests that the Ni p orbitals also gain electron charges upon alloying, further demonstrating that the depleted charge at the Ni site consists primarily of itinerant s electrons. It seems that our calculated s-orbital occupation numbers disagree with the observed depletion of s electrons at the Ni sites. But we would like to mention that in our calculations, s orbitals,

TABLE II. Total integrated number of electrons per atom for the valence orbitals at the Ni and Al sites in Ni_3Al, Ni_3Ga, and reference pure Ni and Al.

	Ni site			Al site	
	n_s	n_p	n_d	n_s	n_p
Ni	0.58(0.02)	0.60(0.03)	8.59(0.03)		
Ni_3Al	0.54(0.04)	0.61(0.03)	8.88(0.03)	1.20(0.02)	1.46(0.02)
Ni_3Ga	0.54(0.02)	0.60(0.03)	8.83(0.02)		
Al				1.51(0.01)	1.48(0.01)

which are different from d orbitals, are extended Bloch orbitals; they are not localized at the atomic sites. In our calculations the local charge neutrality is implicitly guaranteed by the itinerant nature of sp electrons through the screening effect, which is characteristic of metallic systems.

As generally believed, the p-d hybridization effect in transition-metal compounds is closely related to the energy separations between the transition-metal d and the nearest-neighbor (NN) p states as well as the transition-metal-NN bond lengths.[23] Harrison showed that the square of the hybridization coupling constant, V_{pd}^2, is proportional to (r_d^3/d_{NN}^7),[24] where r_d and d_{NN} are the transition-metal d-orbital radius and the transition-metal-NN bond lengths, respectively. The strength of Al(Ga) p-Ni d hybridization in Ni_3Al (Ni_3Ga), which is predominantly determined by the degree of overlap of the participating Ni d and Al(Ga) p orbitals, should be closely associated with the electronic transition probabilities occurring between Ni $3d$- and Al $3p$-(Ga $4p$-) derived states as well as the NN Ni–Al (Ga) bond lengths. To see if this is the case, we obtained the NN bond lengths of 2.54 ± 0.01 Å in Ni_3Al (Ni–Al) and 2.59 ± 0.01 Å in Ni_3Ga (Ni–Ga) using the extended x-ray absorption fine structure (EXAFS) at the Ni K-edge in Ni_3Al and Ni_3Ga, respectively.[25] The NN bond lengths obtained by careful EXAFS analysis give rise to a slightly greater d-p coupling constant in Ni_3Al than in Ni_3Ga. This difference is consistent with the greater size of the Ga atom (covalent radius $= 1.26$ Å) than the Al atom (covalent radius $= 1.18$ Å),[12] which leads to a slightly greater p-d hybridization in Ni_3Al than in Ni_3Ga as predicted by the Harrison's formula. This conclusion is consistent with earlier theoretical calculations, in which Iotova *et al.*[6] obtained slightly smaller d-p energy difference, i.e., $E_d(\mathrm{Ni}) - E_p(\mathrm{X})$, and a slightly larger d-p coupling constant for Ni_3Al than for Ni_3Ga.

V. CONCLUSION

The observed decrease in the intensity of white-line features at Ni L_3 edge and the edge energy shifts towards the lower photon energy at the Ni K-edge XANES relative to that of pure Ni imply an enhancement of Ni $3d$-states filling. The threshold at the Al K-edge XANES for Ni_3Al shifts towards the higher photon energy relative to that of pure Al, which implies that Al loses some p-orbital charges in Ni_3Al. Thus, there is charge transfer from Al $3p$ to Ni $3d$ orbitals. We also found that Ni p orbitals gain some electrons. The property of the local charge neutrality of this metallic system is maintained through the loss of itinerant s electrons at the Ni site to compensate the gain in Ni $4p$ and $3d$ electrons. A prominent feature B_2 observed in the Ni_3Al spectrum at the Al K edge can be attributed to the Al $3p$-derived states, which hybridized strongly with Ni $3d/4sp$ states. Our EXAFS analysis showed that the NN Ni–Al bond length is shorter than that of Ni–Ga. The use of the Harrison's formula indicates that the Ni $3d$ states have a stronger hybridization with the Al $3p$ states in Ni_3Al than with the Ga $4p$ states in Ni_3Ga.

ACKNOWLEDGMENTS

One of the authors (W.F.P.) would like to thank the National Science Council of R.O.C. for financially supporting this research under Contract No. NSC 89-2112-M-032-008. SRRC is also appreciated for the use of their HSGM and wiggler beamlines to perform this study.

[1] N. S. Stoloff, Int. Met. Rev. **29**, 123 (1984).
[2] J. K. Okamoto, C. C. Ahn, and B. Fultz, J. Appl. Phys. **77**, 4380 (1995).
[3] D. A. Muller, S. Subramanian, P. E. Batson, S. L. Sass, and J. Silcox, Phys. Rev. Lett. **75**, 4744 (1995).
[4] Zs. Kovács, L. Kövér, P. Weightman, D. Varga, R. Sanjinés, J. Pálinkás, G. Margaritondo, and H. Adachi, Phys. Rev. B **54**, 8501 (1996).
[5] J. C. Fuggle, F. U. Hillebrecht, R. Zeller, Z. Zolnierek, P. A. Bennett, and Ch. Freiburg, Phys. Rev. B **27**, 2145 (1982).
[6] D. Iotova, N. Kioussis, and S. P. Lim, Phys. Rev. B **54**, 14413 (1996).
[7] D. Hackenbracht and J. Kübler, J. Phys. F **10**, 427 (1980).
[8] S. N. Sun, N. Kioussias, S. P. Lim, A. Gonis, and W. H. Gourdin, Phys. Rev. B **52**, 14421 (1995).
[9] L. S. Hsu, K. L. Tsang, and S. C. Chung, Mater. Res. Soc. Symp. Proc. **437**, 53 (1996).
[10] R. V. Kasowski, M.-H. Tsai, T. N. Rhodin, and D. D. Chambliss, Phys. Rev. B **34**, 2656 (1986); M.-H. Tsai and K. C. Hass, *ibid.* **51**, 14616 (1995); K. C. Hass, M.-H. Tsai, and R. V. Kasowski, *ibid.* **53**, 44 (1996).
[11] *International Tables for X-Ray Crystallography*, edited by N. F. M. Henrand and K. Lonsdal (Kynoch, Birmingham, 1969), Vol. I.
[12] *Table of Periodic Properties of the Elements* (Sargent-Welch Scientific Company, Skokie, IL, 1980).
[13] D. J. Chadi and M. L. Cohen, Phys. Rev. B **8**, 5747 (1973).
[14] H. J. Monkhorst and J. D. Pack, Phys. Rev. B **13**, 5188 (1976).
[15] G. van der Laan, J. Zaanen, G. A. Sawatzky, R. Karnatak, and J. M. Esteva, Phys. Rev. B **33**, 4253 (1986); G. van der Laan, B. T. Thole, G. A. Sawatzky, and M. Verdaguer, *ibid.* **37**, 6587 (1988).
[16] E. Tamura, J. van Ek, M. Fröba, and J. Wong, Phys. Rev. Lett. **74**, 4899 (1995).
[17] M. Kuhn and T. K. Sham, Phys. Rev. B **49**, 1647 (1994); I. Coulthard and T. K. Sham, Phys. Rev. Lett. **77**, 4824 (1996).
[18] T. K. Sham, A. Hiraya, and M. Watanabe, Phys. Rev. B **55**, 7585 (1997).
[19] H. H. Hsieh, Y. K. Chang, W. F. Pong, J. Y. Pieh, P. K. Tseng, T. K. Sham, I. Coulthard, S. J. Naftel, J. F. Lee, S. C. Chung, and K. L. Tsang, Phys. Rev. B **57**, 15204 (1998).
[20] See Appendix B, *Unoccupied Electronic States*, edited by J. C. Fuggle and J. E. Inglesfield (Springer, Berlin, 1992).
[21] D. A. Muller, D. J. Singh, and J. Silcox, Phys. Rev. B **57**, 8181 (1998).
[22] D. A. Muller, P. E. Batson, and J. Silcox, Phys. Rev. B **58**, 11970 (1998).
[23] B. E. Larson, K. C. Hass, H. Ehrenreich, and A. E. Carlsson, Phys. Rev. B **37**, 4137 (1988).
[24] W. A. Harrison, *Electronic Structure and the Properties of Solids* (Freeman, San Francisco, 1980).
[25] W. F. Pong *et al.* (unpublished).

Structural characterization of the Co/Cr multilayers by x-ray-absorption spectroscopy

Y. H. Liou,[1] W. F. Pong,[1,*] M.-H. Tsai,[2] K. H. Chang,[1] H. H. Hseih,[1] Y. K. Chang,[1] F. Z. Chien,[1] P. K. Tseng,[1] J. F. Lee,[3] Y. Liou,[4] and J. C. A. Huang[5]

[1]*Department of Physics, Tamkang University, Tamsui 251, Taiwan*

[2]*Department of Physics, National Sun Yat-Sen University, Kaohsiung 804, Taiwan*

[3]*Synchrotron Radiation Research Center, Hsinchu Science-based Industrial Park, Hsinchu 300, Taiwan*

[4]*Institute of Physics, Academic Sinica, Taipei 115, Taiwan*

[5]*Department of Physics, National Cheng Kung University, Tainan 701, Taiwan*

(Received 11 November 1999; revised manuscript received 4 May 2000)

We have performed Cr and Co *K*-edge x-ray-absorption measurements to investigate the dependence of local electronic and atomic structures on the Cr-layer thickness in epitaxial Co(1 $\bar{1}$00) (40 Å)/Cr(211) (t_{Cr}) (t_{Cr} = 2, 3, 5, 7, and 9 Å) multilayers. The Cr *K* x-ray-absorption near-edge fine structure (XANES) spectra of the Co/Cr multilayers indicate an abrupt transition of the Cr layer from hcp to bcc structure when the thickness of the Cr layer is increased to exceed ~5 Å or three atomic layers. Our results offer an upper limit for the ability of the Co/Cr interface to stabilize the hcp structure in the thin Cr layer. The numbers of nearest-neighbor and next-nearest-neighbor atoms in the Cr and Co layers determined by extended x-ray-absorption fine-structure measurements performed at the Cr and Co *K* edge, respectively, are consistent with the XANES results.

Magnetic multilayers have attracted a great deal of attention over the last decade because of their peculiar magnetic properties and their technological and fundamental importance.[1] The oscillatory variation of the interlayer exchange coupling with respect to the separation between two ferromagnetic layers in the multilayer systems is particularly of interest.[2] For epitaxial Co/Cr multilayers, previous works showed that the magnetic properties have the characteristics of giant and anisotropic magnetoresistance.[3–5] It was also found that the magnetic and magnetotransport properties of the magnetic multilayers are strongly affected by their electronic and atomic structures.[6] The reflection high-energy electron diffraction (RHEED) analyses by Vavra *et al.*[7] and Henry *et al.*[8] showed that the Cr layer in epitaxial Co/Cr multilayers exhibited an abrupt transition from bcc structure to close-packed structure (fcc or hcp) at a Cr-layer thickness of $\leqslant$ 5 Å. This property was attributed to the interfacial energy that stabilizes the thermodynamically less favored densest atomic arrangement. However, they obtained different local atomic structures around Cr when the Cr layer is very thin. Vavra *et al.* found that pseudomorphically grown Cr layers are constrained coherently to the hcp structure of the underlying Co, while Henry *et al.* reported that no pseudomorphism occurs at the Cr/Co interface, but it is more likely that interdiffusion resulted in forming a close-packed CoCr alloy. Another investigation also found the existence of interdiffusion at the Cr/Co interface of the sputtering grown Co/Cr multilayers.[9,10] Different orientations and preparation conditions of the thin-film samples used in these studies might be the cause of the different interfacial structures. The mismatch of the atomic arrangement at the interface depends on the orientation of the multilayers. Recently, based on structural characterization Huang *et al.*[3] found that though bcc and hcp structures have different atomic arrangements, Co(1 $\bar{1}$00) and Cr(211) planes match extremely well in symmetry and lattice parameters. In this crystal orientation, the existence of fcc Co/Cr-alloy structure at the interface may not be likely because the fcc structure is incompatible with either hcp(1 $\bar{1}$00) or bcc(211) atomic arrangement. The x-ray-absorption spectrum is very sensitive to the local environment around the absorbing atom, which can be used as a fingerprint of the crystallographic structure and allows us to study the local structures in multilayer systems.[11,12] In this work we measure the local electronic and atomic structures of a series of Co/Cr multilayers and characterize the variation of local electronic and atomic structures with respect to the Cr-layer thickness. This study may help us understand the dependence of the local electronic and atomic structures in the epitaxial Co/Cr multilayers on the Cr-layer thickness.

X-ray absorption spectra of the Co/Cr multilayers were measured using a double-crystal Si(111) monochromator at the wiggler beamline, with an electron-beam energy of 1.5 GeV and a maximum stored current of 200 mA at the Synchrotron Radiation Research Center (SRRC) in Hsinchu, Taiwan. The absorption spectra of the Co/Cr multilayers and thin-film CoCr alloy at the Cr and Co *K* edges were measured using the fluorescence mode with the Lytle detector at room temperature. The spectra of the reference Cr and Co foils were obtained in transmission mode. All the spectra were collected with step energy of 0.5 eV in the x-ray-absorption near-edge structure (XANES) region and of 2 eV in the extended x-ray-absorption fine-structure (EXAFS) region. Samples of $24x$[Co (40 Å)/Cr (2 Å)] and $20x$[Co (40 Å)/Cr (t_{Cr})] multilayers with t_{Cr}=3, 5, 7, and 9 Å and a ~50 Å Mo buffer were deposited on the MgO(110) substrates. X-ray-diffraction results indicate that the Co and Cr layers deposited in the alternating Co/Cr multilayers mainly have hcp/bcc structure in the Co(1 $\bar{1}$00)/Cr(211) orientation. The details of the preparation of the Co/Cr multilayers and x-ray-diffraction determination of the orientation of these multilayers have been described elsewhere.[3–5]

Figures 1 and 2 show, respectively, the Cr and Co *K*-edge XANES spectra obtained for the Co/Cr multilayers, refer-

 ©2000 The American Physical Society

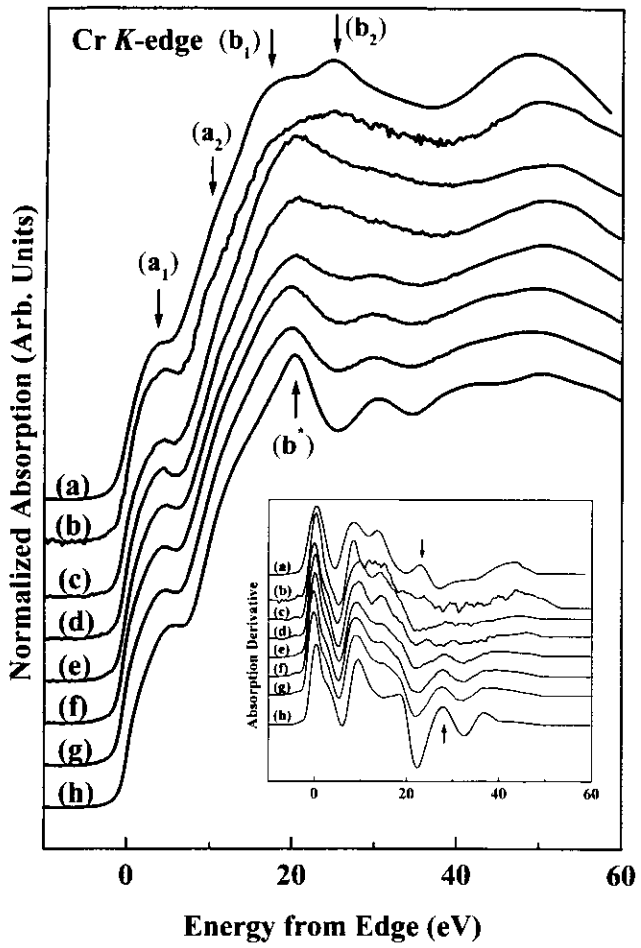

FIG. 1. Normalized Cr K near-edge absorption spectra for epitaxial Co (40 Å)/Cr (t_{Cr}) (t_{Cr}=2, 3, 5, 7, and 9 Å) multilayers. (a) Co foil (offset Co K edge), (b) CoCr alloy, (c) t_{Cr}=2 Å, (d) t_{Cr} =3 Å, (e) t_{Cr}=5 Å, (f) t_{Cr}=7 Å, (g) t_{Cr}=9 Å, and (h) Cr foil.

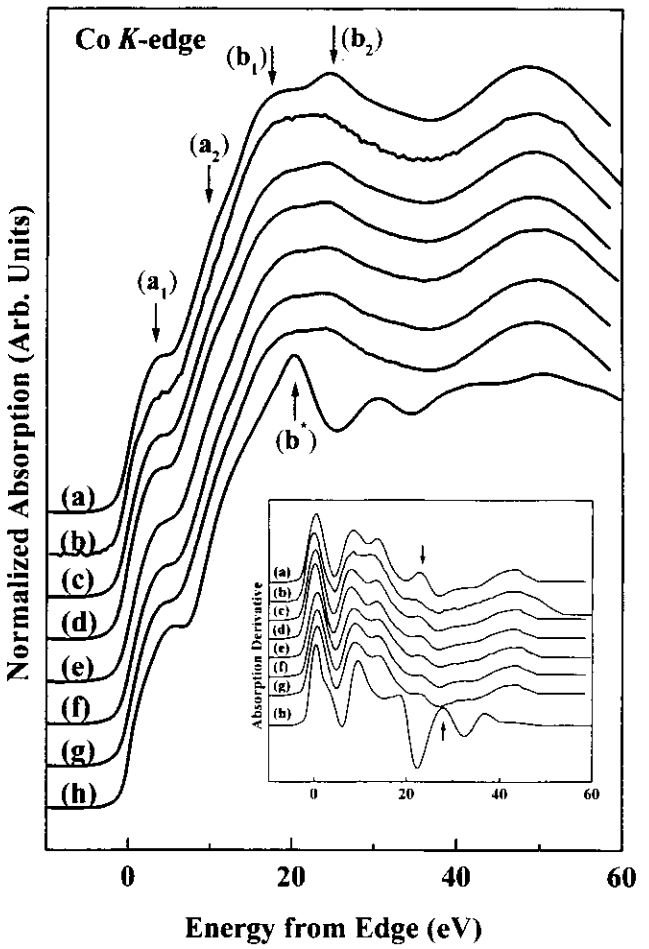

FIG. 2. Normalized Co K near-edge absorption spectra for epitaxial Co (40 Å)/Cr (t_{Cr}) (t_{Cr}=2, 3, 5, 7, and 9 Å) multilayers. (a) Co foil, (b) CoCr alloy, (c) t_{Cr}=2 Å, (d) t_{Cr}=3 Å, (e) t_{Cr}=5 Å, (f) t_{Cr}=7 Å, (g) t_{Cr}=9 Å, and (h) Cr foil (offset Cr K edge).

ence CoCr alloy, and Cr and Co foils. For all the spectra, zero energy was selected at the inflection point of the threshold in the spectra. The zero energies correspond to absolute energies of 5989.0 and 7709.1 eV, respectively, for the Cr and Co K edges. Due to the bulk sensitivity of fluorescence measurements, the spectra in Figs. 1 and 2 predominantly reflect the bulk absorption of the Co/Cr multilayers. The normalized EXAFS oscillations $\chi(k)$ are weighted by k^3 for both Cr and Co K edges, and the corresponding Fourier transforms (FTs) of the $k^3\chi$ data for the Co/Cr multilayers and reference samples are shown in Figs. 3 and 4, respectively. Further analysis involved the use of a combination of the multiple-scattering EXAFS computer program FEFF6 (Ref. 13) and the nonlinear least-squares-fitting computer program FEFFIT.[14] As also shown in Figs. 3 and 4, the quality of the fit for the nearest-neighbor (NN) and next-nearest-neighbor (NNN) bond lengths is quite good.

The part of the Cr K-edge XANES spectra of the Co/Cr multilayers, reference CoCr alloy, and Cr foil and of the offset Co K-edge XANES spectra of the Co foil between labels b_1 and b_2 as shown in Fig. 1 can be attributed to the dipole $1s$-to-$4p$ transitions above the Fermi level. The two small bumps in the region from about 0 to 10 eV above the edge (labeled as a_1 and a_2) are primarily due to the Cr and Co $1s$-to-$3d$ transition through the Cr and Co p-d rehybridization.[15] The two-peak features b_1 and b_2 (labeled by vertical arrows) in the Cr K-edge XANES of the Co/Cr multilayers with a Cr-layer thickness t_{Cr} less than 5 Å closely resemble those of the Co foil with a hcp structure. In contrast, the single-peak feature in the Cr K-edge spectra of the Co/Cr multilayers with $t_{Cr}>5$ Å resembles the single sharp feature b^* located in the region between peaks b_1 and b_2 in the spectrum of the Cr foil with a bcc structure. The features in the Cr K-edge XANES of the CoCr alloy are much broader and appear to be least resolved in comparison with those of the Co/Cr multilayers and Cr and Co foils. The first derivatives of the XANES spectra of the Co/Cr multilayers, CoCr alloy, and Cr and Co foils are shown in the inset of Fig. 1. A general trend of the change from the single peak b^* to the double peaks b_1 and b_2 can be easily seen when the Cr-layer thickness decreases in the Co/Cr multilayers. This trend clearly indicates a local structural transition at $t_{Cr}\sim 5$ Å in the Co/Cr multilayers. It may suggest that pseudomorphic Cr films can be grown on Co and can be constrained coherently into the hcp structure in thin layers ($t_{Cr}<5$ Å). In contrast, the Cr layer prefers to be bulk like when its thickness is greater than 5 Å. The intensity of bumps a_1 and a_2 in the Cr K-edge XANES spectra remains nearly constant. The Co K-edge XANES spectra of the Co/Cr multilayers shown in Fig. 2 contain relatively well-

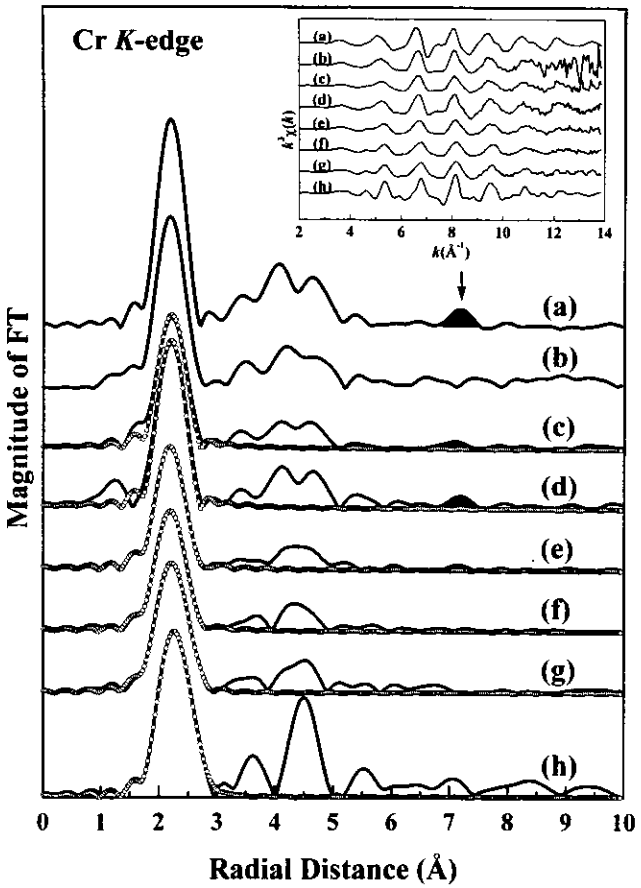

FIG. 3. Fourier transform amplitudes of the EXAFS $k^3\chi$ data at the Cr K edge for Co/Cr multilayers. (a) Co foil, (b) CoCr alloy, (c) t_{Cr}=2 Å, (d) t_{Cr}=3 Å, (e) t_{Cr}=5 Å, (f) t_{Cr}=7 Å, (g) t_{Cr}=9 Å, and (h) Cr foil. Final fit of theory to the NN and NNN bond lengths (open circles). The inset represents the Cr K-edge EXAFS oscillation $k^3\chi$ data. In fitting a model compound to the experimental EXAFS, the coordination number of NN Co was fixed at 12 for $t_{Cr}<5$ Å with a hcp structure, while the coordination numbers of NN Cr and NNN Cr were fixed at 8 and 6, respectively, for $t_{Cr}>5$ Å with a bcc structure.

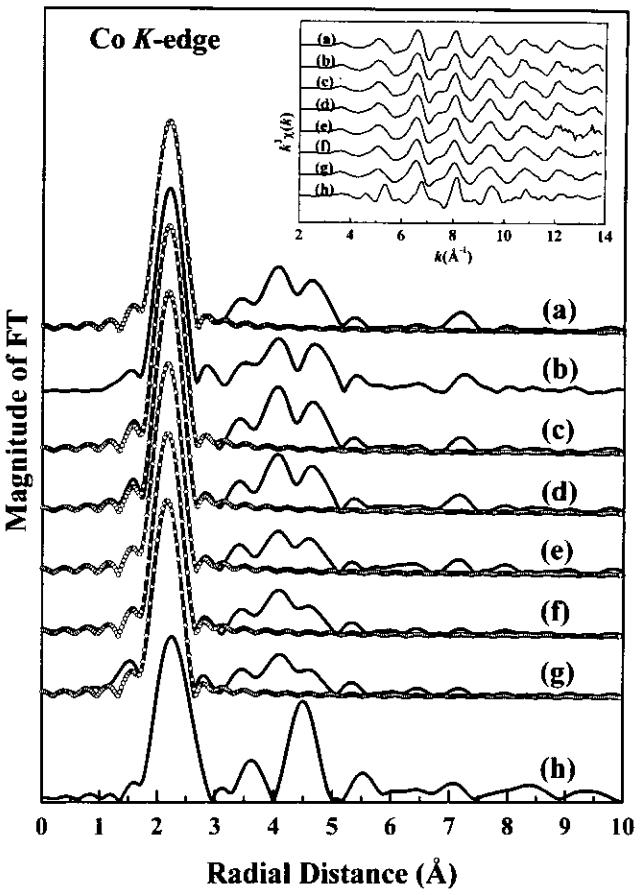

FIG. 4. Fourier transform amplitudes of the EXAFS $k^3\chi$ data at the Co K edge for Co/Cr multilayers. (a) Co foil, (b) CoCr alloy, (c) t_{Cr}=2 Å, (d) t_{Cr}=3 Å, (e) t_{Cr}=5 Å, (f) t_{Cr}=7 Å, (g) t_{Cr}=9 Å, and (h) Cr foil. Final fit of theory to the NN bond lengths (open circles). The inset represents the Co K-edge EXAFS oscillation $k^3\chi$ data. The coordination number of Co was fixed at 12 in fitting a model compound to the experimental EXAFS because of a very small contribution from Cr atoms.

resolved two-peak features b_1 and b_2, which resemble those of the Co foil. The first derivatives of the Co K-edge XANES spectra of the Co/Cr multilayers, CoCr alloy, and Co and Cr foils are also shown in the inset of Fig. 2.

Figures 3 and 4 show the Cr and Co K-edge FTs of the $k^3\chi$ data for the Co/Cr multilayers, CoCr alloy, and Cr and Co foils. The first peaks in the FT spectra shown in Fig. 3 appear to have roughly the same location, though they have different heights and full widths at the half maximum. However, the peaks at a distance larger than ~3 Å appear to differ significantly and can be attributed to differences in the average environment in farther away shells between the two $t_{Cr}>5$ Å and $t_{Cr}\leq 5$ Å cases. The features in the FT spectra of the Co/Cr multilayers with a thick Cr layer ($t_{Cr}>5$ Å) have a single peak near 4.5 Å. They resemble closely that of the Cr foil with a bcc structure.[11] On the other hand, the local atomic structures of thin Cr layers ($t_{Cr}\leq 5$ Å) in the Co/Cr multilayers and CoCr alloy are quite similar to that of the Co foil with a hcp structure. In the region between 6.8 and 7.3 Å in the FT spectra shown in Figs. 3(a) and 3(c)–3(e), the spectra have a common feature marked by shaded peaks. Other spectra do not have this feature. Since the spectra of Figs. 3(a) and 3(c)–3(e) belong to the Co foil and Co/Cr multilayers with thin Cr layers ($t_{Cr}\leq 5$ Å), respectively, our FT spectra show that the thin Cr layers ($t_{Cr}\leq 5$ Å) are more likely to have the same hcp structure of the Co foil. This agrees with XANES results and further confirms that the epitaxially grown $t_{Cr}\sim 5$ Å Cr layers in the Co/Cr multilayers are constrained to be Co metal like as reported by earlier RHEED studies.[7,8] The similarity between the XANES spectra of the reference CoCr alloy and Co metal suggests that the CoCr alloy has a hcp structure, in agreement with our x-ray-diffraction measurement. The FT spectra shown in Fig. 3 have the characteristic of splitting two-neighbor shells in the region between 3.8 and 5.0 Å for $t_{Cr}\leq 5$ Å. The splitting two-neighbor shells are also found in the FT spectra of the Co K edge for the Co/Cr multilayers, CoCr alloy, and Co foil as shown in Fig. 4. In Fig. 4 the splitting two-neighbor shells are nearly at the same position for the Co/Cr multilayers, CoCr alloy, and Co foil, but the heights are obviously larger for thinner Cr layers than for thicker Cr layers in the Co/Cr multilayers. This property can be primarily attributed to the decrease of the structural order due to NNN bond-length dis-

tortion in the Co layer caused by the thick bcc Cr layer.

A best-fit procedure is applied to the first main peaks in the Cr *K*-edge EXAFS FT spectra to obtain NN and NNN bond lengths using the one- and two-shell models for t_{Cr} <5 Å and $t_{Cr}>5$ Å, respectively. The Cr atoms are found bonded with 12 NN Co atoms at 2.50 ± 0.01 Å, which is a characteristic of the hcp structure, for $t_{Cr}<5$ Å. For t_{Cr} >5 Å, the Cr atoms are bonded with 8 NN Cr atoms at 2.49 ± 0.01 Å and 6 NNN Cr atoms at 2.78 ± 0.02 Å for t_{Cr} $=7$ Å and at 2.84 ± 0.02 Å for $t_{Cr}=9$ Å indicative of a bcc structure. The 2.84 Å NNN bond length is close to that of the bulk Cr metal of 2.88 Å. For $t_{Cr}=5$ Å the Cr layer contains ~3 atomic layers of Cr. The central Cr layer is sandwiched between two Cr side layers, so that the nearest neighbors of the atoms in this layer are all Cr atoms. On the other hand, the side-layer Cr atoms have some bcc-type Cr nearest neighbors and some hcp-type Co nearest neighbors. The real sample may even contain both hcp and bcc phases. Thus, in this case, the EXAFS data were fitted with a combination of 1/3 hcp and 2/3 bcc coordinations. The NN and NNN bond lengths obtained are 2.50 ± 0.01 and 2.84 ± 0.02 Å, respectively. They are consistent with those determined for other Cr-layer thicknesses. The single-shell model is fitted for the first main peak of the Co *K*-edge FT spectra for all Co/Cr multilayers. The Co atoms are found bonded with 12 NN Co atoms at 2.49–2.50 Å indicative of a hcp structure.

Transition metals with a fcc structure have a closed or nearly closed outermost *d* shell, while those with a hcp structure have a few singly occupied *d* orbitals.[16] Both fcc and hcp structures are the densest structure, in which each atom has 12 NN atoms and the coupling between atoms are dominated by metallic bonding through itinerant electrons, which are not directional. In contrast, the transition metals with a bcc structure have from 3 to 6 *d* electrons in the outermost *d* shell. Since the 5 *d* orbitals are directional, the contribution of *d* orbitals to the coupling between two neighboring atoms is also directional, which renders the bcc structure with a smaller coordination number of 6 becomes more favorable than the fcc/hcp structure. When the Cr layers are one and two atoms thick and have the hcp $(1\bar{1}00)$ structure of the Co layer, the Cr atoms are coordinated, respectively, with 10 and 8 or 6 Co atoms, which couple with the Cr atoms through itinerant electrons and stabilize the hcp structure. For a three-atom-thick Cr layer, the Cr atoms are coordinated with more Cr atoms than Co atoms; the additional directional Cr-Cr couplings through *d* orbitals render the bcc structure to become more favorable. Based on the above argument, the observed ultrathin (three-atomic-layer) critical thickness of the bcc Cr layer seems to suggest that the interdiffusion of Co and Cr atoms at the interface is less likely or at least is limited to very few layers. The physical reason is that interdiffusion reduces the number of Cr atoms surrounding a given Cr atom and tends to destabilize the bcc structure, so that a thicker Cr layer is required to be stabilized in the bcc structure. Based on structural characterization, Huang *et al.*[3] found that though bcc and hcp structures have different atomic arrangements, Co$(1\bar{1}00)$ and Cr(211) planes match extremely well in symmetry and lattice parameters. The unit cell of Co$(1\bar{1}00)$, 4.07 Å×2.51 Å, matches perfectly that of Cr(211), 4.07 Å×2.50 Å. The one-atom-thick hcp Cr$(1\bar{1}00)$ layer is expected to have a similar excellent match and have negligible strain energy. For the two-atom-thick hcp Cr$(1\bar{1}00)$ layer, the strain energy is associated with the distortion of the NN bond angles from those of the bcc Cr(211) structure. For semiconductors the NN bonding is covalent and directional and the bond-angle distortion gives rise to significant strain energy.[17] In contrast, for transition metals the strain energy associated with the bond-angle distortion is given rise by directional *d*-orbital couplings, which is not as significant as the nondirectional metallic bonding through itinerant electrons. Thus the strain energy in the two-atom-thick hcp Cr$(1\bar{1}00)$ layer is of second order. During the deposition of the third Cr layer, this strain energy can be easily overcome by the energy transferred from the adsorption energy of the approaching gas-phase Cr atoms. Thus a three-atom-thick bcc Cr(211) layer can be easily formed.

In summary, our Cr and Co *K*-edge XANES measurements for the epitaxial Co (40 Å)/Cr (t_{Cr}) ($t_{Cr}=2$, 3, 5, 7, and 9 Å) multilayers show an abrupt transition of the Cr layer from hcp structure to bcc structure at ~5 Å. Our results offer an upper limit for the ability of the Co/Cr interface to stabilize the hcp structure in the thin Cr layer. The hcp-to-bcc transition around $t_{Cr}\sim5$ Å is further confirmed by the EXAFS measurements performed at the Cr and Co *K* edge.

One of the authors (W.F.P.) would like to thank the National Science Council of R.O.C. for financially supporting this research under Contract No. NSC 89-2112-M-032-008. SRRC is also appreciated for the use of their wiggler beamline to perform this study.

*Author to whom correspondence should be addressed.

[1] *Ultrathin Magnetic Structures*, edited by J. A. C. Bland and B. Heinrich (Springer-Verlag, Berlin, 1994), Vols. I and II.

[2] S. S. P. Parkin, N. More, and K. P. Roche, Phys. Rev. Lett. **64**, 2304 (1990); M. T. Johnson, R. Coehoorn, J. J. de Vries, N. W. E. McGee, J. aan de Stegge, and P. J. H. Bloemen, *ibid.* **69**, 969 (1992).

[3] J. C. A. Huang, Y. Liou, Y. D. Yao, W. T. Yang, C. P. Chang, S. Y. Liao, and Y. M. Hu, Phys. Rev. B **52**, R13 110 (1995).

[4] J. C. A. Huang, F. C. Tang, W. W. Fang, R. L. Liu, Y. M. Hu, C. K. Lo, Y. Liou, Y. D. Yao, W. T. Yang, C. P. Chang, and S. Y. Liao, J. Appl. Phys. **79**, 4790 (1996).

[5] Y. D. Yao, Y. Liou, J. C. A. Huang, S. Y. Liao, I. Klik, W. T. Yang, C. P. Chang, and C. K. Lo, J. Appl. Phys. **79**, 6533 (1996).

[6] G. A. Prinz, Phys. Rev. Lett. **54**, 1051 (1985); D. P. Pappas, K. P. Kämper, and H. Hopster, *ibid.* **64**, 3179 (1990); E. E. Fullerton, D. M. Kelly, J. Guimpel, I. K. Schuller, and Y. Bruynseraede, *ibid.* **68**, 859 (1992).

[7] W. Vavra, D. Barlett, S. Elagoz, C. Uher, and R. Clarke, Phys. Rev. B **47**, 5500 (1993).

[8] Y. Henry, C. Mény, A. Dinia, and P. Panissod, Phys. Rev. B **47**, 15 037 (1993).

[9] N. Sato, J. Appl. Phys. **61**, 1979 (1987).

[10] P. Boher, F. Giron, Ph. Houdy, P. Beauvillain, C. Chappert, and P. Veillet, J. Appl. Phys. **70**, 5507 (1991).

[11] S. Pizzini, F. Baudelet, D. Chandesris, A. Fontaine, H. Magnan, J. M. George, F. Petroff, A. Barthélemy, A. Fert, R. Loloee, and P.

A. Schroeder, Phys. Rev. B **46**, 1253 (1992); S. Pizzini, F. Baudelet, A. Fontaine, M. Galtier, D. Renard, and C. Marlière, *ibid.* **47**, 8754 (1993).

[12] P. Le Fevre, H. Magnan, O. Heckmann, V. Briois, and D. Chandesris, Phys. Rev. B **52**, 11 462 (1995); P. Le Fevre, H. Magnan, and D. Chandesris, Surf. Sci. **352–354**, 923 (1996).

[13] J. J. Rehr, J. M. deLeon, S. I. Zabinsky, and R. C. Albers, J. Am. Chem. Soc. **113**, 5135 (1991); J. J. Rehr, R. C. Albers, and S. I. Zabinsky, Phys. Rev. Lett. **69**, 3397 (1992).

[14] A. I. Frenkel, E. A. Stern, M. Qian, and M. Newville, Phys. Rev. B **48**, 12 449 (1993).

[15] T. K. Sham, A. Hiraya, and M. Watanabe, Phys. Rev. B **55**, 7585 (1997).

[16] *Table of Periodic Properties of the Elements* (Sargent-Welch Scientific, Skokie, IL, 1990).

[17] W. A. Harrison, *Electronic Structure and the Properties of Solids* (Freeman, San Francisco, 1980).

第十屆鑽石研究國際會議

彭維鋒
（淡江大學物理系）

一九九九年第十屆鑽石研究國際會議於9月12日至9月17日在捷克布拉格舉行。會議以鑽石與類鑽石相關研究為討論主題，在此主題下又可分為鑽石樣品成長、實驗技術、奈米碳管、鑽石應用及相關材料等研究子題。由於此國際會議每年舉行一次，可視為鑽石研究應用於材料相關討論會中最為重要之學術研討會議，故國際相關研究人員均甚踴躍參加此次會議。在此次會議中共有各類口頭宣讀論文及壁報展示。由於參加人員主要來自歐、美、日等主要科技先進國家，本人口頭宣讀論文是有關利用同步輻射X吸收光譜矽-碳-氮化合物之研究。

基本上由於八十年代同步輻射技術漸臻成熟及歐美日大力發展，及建造更先進同步輻射加速器，因此利用同步輻射為光源作相關化學、物理、材料、生物及醫學研究，已逐漸取代傳統X光機光源。此次六天的會議，筆者深感歐美日各國對於利用同步輻射光源X光吸收光譜對相關鑽石材料之研究投入相當多人力及經費，亦有相當不錯的成果。而利用同步輻射光源作相關研究在台灣尚屬起步，但台灣同步輻射有相當優異的第三代光源，如果能善加利用則相信未來在國際同步輻射研究台灣的研究群將能扮演相當積極角色。在此筆者並感謝國科會經費補助得以參加此次會議。

攜回資料：Diamond 99 會議摘要

Electronic and atomic structures of Si-C-N thin film by x-ray-absorption spectroscopy

W. F. Pong[1,*], Y. K. Chang[1], H. H. Hsieh[1], M.-H. Tsai[2], K. H. Lee[1], T. E. Dann[1,3]

F. Z. Chien[1], P. K. Tseng[1], K. L. Tsang[3], W. K. Su[4]

L. C. Chen[5], S. L. Wei[5], K. H. Chen[6], D. M. Bhusari[6], Y. F. Chen[7]

(1) Department of Physics, Tamkang University, Tamsui, Taiwan 251, Republic of China

(2) Department of Physics, National Sun Yat-Sen University, Kaohsiung, Taiwan 804, Republic of China

(3) Synchrotron Radiation Research Center, Hsinchu, Taiwan 300, Republic of China

(4) Department of Applied Physics, Chung-Cheng Institute of Technology, Ta-Hsi, Taiwan 335, Republic of China

(5) Center for Condensed Matter Sciences, National Taiwan University, Taipei, Taiwan 107, Republic of China

(6) Institute of Atomic and Molecular Sciences, Academia Sinica, Taipei, Taiwan 107, Republic of China

(7) Department of Physics, National Taiwan University, Taipei, Taiwan 107, Republic of China

* Author to whom all correspondence should be addressed

Abstract

This study measures X-ray absorption spectra of crystalline (*c*)-Si-C-N thin film at the C and Si *K*-edge using the sample drain current mode, and at the N *K*-edge using the fluorescent mode. A resonance peak resembling the C 1*s* core exciton in CVD-diamond/Si is observed. And a broad feature occurring in the energy range between ~290 and 300 eV can be assigned to the antibonding C 2*p*-Si 3*sp* hybridized states and the C 2*p*-N 2*sp* hybridized states as well. Analysis of the N *K*-edge near edge absorption spectra reveals a similar feature in *c*-Si-C-N and α-Si_3N_4, suggesting that nitrogen atoms generally have similar local environment in these two materials. Moreover, results obtained from Si *K*-edge absorption spectra for *c*-Si-C-N demonstrate a proportional combination of local Si-N and Si-C bonds, associated with the local tetrahedral C-Si-N_3 as well as the long-range ordered atomic structure around Si atoms.

Keywords: x-ray absorption near-edge structure (XANES); extended x-ray absorption fine structure (EXAFS); thin film; core exciton; hybridized states; first-principles calculations

TEL: +886-2-625-2333, FAX: +886-2-625-2316

e-mail: pong@exafs.phys.tku.edu.tw

1. INTRODUCTION

It is well known, silicon carbide (Si-C) and silicon nitride (Si-N) are highly promising for wide applications in mechanics, optics, and electronics.[1] Carbon nitride (C-N), another binary compound, has recently also received extensive attention owing to its potential applications in new hard materials.[2] The importance of Si-C and Si-N as well as the hypothetical C-N binary systems suggested that the ternary Si-C-N system may be similarly importance. However, detailed analyses of the local electronic and atomic structures of this ternary system have seldom been performed. Recently, Gheorghiu *et al.*[3] and Ténégal *et al.*[4] have reported Si *K*-edge extended x-ray absorption fine structure (EXAFS) studies of nanometric Si-C-N powders. However, they obtained different atomic structures, Gheorghiu *et al.* suggested the existence of a local C-Si-N_3 arrangement around Si atoms, which is in contrast to the Si atoms randomly linked together through C-N network proposed by Ténégal *et al.*. Trying to clarify this discrepancy, we have performed an analysis of C, N, and Si *K*-edge x-ray absorption spectra for the *c*-Si-C-N thin film.

2. EXPERIMENT

The C, N, and Si *K*-edge x-ray absorption spectra of the *c*-Si-C-N thin film with that of chemical-vapor-deposition (CVD)-grown diamond on Si substrate, α-Si_3N_4 powders, and thin film β-SiC and *c*-Si(100) as references were measured using the high-energy spherical grating monochromator (HSGM) and InSb(111) double crystal monochromator (DCM) beamlines, with an electron-beam energy of 1.5 GeV and a

maximum stored current of 200 mA at the Synchrotron Radiation Research Center (SRRC), Hsinchu, Taiwan. The spectra for C and Si *K*-edge were measured using the sample drain current mode. The fluorescence measurements for N *K*-edge spectra were taken with a high-sensitivity seven-element Ge detector at room temperature. The *c*-Si-C-N sample was grown by microwave plasma-enhanced chemical vapor deposition process on a crystalline Si(100) substrate. Details of the preparation procedure for similar compounds can be found elsewhere.[5]

3. RESULTS AND DISCUSSION

Figure 1 illustrates the C *K*-edge x-ray absorption near edge structure (XANES) spectra of β-SiC, *c*-Si-C-N, and CVD-grown diamond on Si substrate (abbreviated hereafter Diamond/Si) for comparison. According to this figure, the spectra of Diamond/Si clearly display a sharp feature closely resembling that reported in earlier works.[6] The spike of the C 1*s* core exciton resonance at ~289.2 eV and a relatively broad sp^3 bonded carbon of σ* features occur between 290 and 302 eV. The relatively small peak at ~285 eV of Diamond/Si obviously appears due to nondiamond-like sp^2 bonded carbon of π* states.[7] On the other hand, the C 1*s* core exciton resonance of β-SiC displays a relatively broader feature than that of the Diamond/Si. We attribute the main broader feature of the near-edge region in β-SiC to dipole-allowed transitions of photoelectrons from C 1*s* states to unoccupied 2*p* states, which have been hybridized significantly with the Si 3*sp* states according to the calculated density of states for β-SiC.[8] Meanwhile, we infer, as for the case of Diamond/Si, that the

relatively broad resonance peak of the *c*-Si-C-N can also be attributed to the C 1*s* core excitonic state. Furthermore, based on results of the first-principles calculations using the pseudofunction method,[9] the pre-edge π^*-like peak and the broad feature occurring in the energy range between ~290 and 300 eV on the C *K*-edge spectra of *c*-Si-C-N, can also be assigned to the antibonding C 2*p*-Si 3*sp* hybridized states and the C 2*p*-N 2*sp* hybridized states as well.

Figure 2 displays the photon-flux-normalized N *K*-edge XANES spectra of the *c*-Si-C-N film and α-Si_3N_4 powders. This figure shows a splitting double-peak features near 406.0 and 403.8 eV in the α-Si_3N_4 spectrum. Based on the calculated density of states for N 2*p* symmetry,[10] the double-peak at N *K*-edge spectra of α-Si_3N_4 can be attributed to antibonding N 2*p*-Si 3*p* and N 2*p*-Si 3*s* hybridized states. In addition, our experimental results indicate a nearly identical spectra between *c*-Si-C-N and α-Si_3N_4, implying that nitrogen atoms clearly have similar local environment in both *c*-Si-C-N and α-Si_3N_4. Consequently, the white line features at the N *K*-edge spectra of the *c*-Si-C-N can be assigned primarily to the antibonding N 2*p*-Si 3*sp* hybridized states and the N 2*p*-C 2*sp* hybridized states.[9]

Figure 3 displays the photon-flux-normalized Si *K*-edge XANES spectra for *c*-Si(100), *c*-Si-C-N, α-Si_3N_4, and β-SiC. In the case of *c*-Si(100), the Si *K*-edge XANES spectrum reflects transition from the Si 1*s* core level to unoccupied Si 3*p*-derived states. This figure also displays characteristic double-peak features (labeled as two vertical dashed lines) above the edge and its approximate 1.0 eV energy separation. Figure 3 also clearly exhibits that the threshold in the Si *K*-edge XANES of

c-Si-C-N film shifts toward higher binding energies, and the general lineshape of the spectra distinctly differs from that of *c*-Si(100). This observation reveals that the chemical states of the absorbing silicon atoms within *c*-Si-C-N are obviously altered in comparison with that of *c*-Si(100), and no segregation of silicon atoms or silicon atoms occurs for the local Si-Si bonds in the *c*-Si-C-N. Furthermore, as seen in Fig. 3, the Si *K*-edge XANES spectra for *c*-Si-C-N and α-Si_3N_4 are shown quite similar, both consist of main peak (labeled A) and accompanied a shoulder (labeled B). However, the *c*-Si-C-N spectrum has a more prominent peak B and peaks A and B appear to be well resolved. We suggest that the prominent peak B in *c*-Si-C-N could be due to the existence of local Si-C bonds around silicon atoms so that the energy position of peak B is quite close to that of the maximum peak of β-SiC, which is supported by the result of C *K*-edge XANES that indicates the occurrence of local C-Si bonds in *c*-Si-C-N and our theoretical calculations[9]. In order to precisely determine the local environment around silicon atoms and to verify the conclusions deriving from the C, N, and Si *K*-edge XANES spectra for the *c*-Si-C-N as discussed above, the Si *K*-edge EXAFS spectra were measured from *c*-Si-C-N using the sample drain current mode at room temperature.[11] We found that the Si atoms are bounded with 3 Si-N and Si-C bonds. Thus, the local atomic structure of *c*-Si-C-N, on average, is quite similar to that of the tetrahedral C-Si-N_3 arrangement and its crystal structure is likely α-Si_3N_4 phase, which further confirms the conclusions deriving from the C, N, and Si *K*-edge XANES spectra for the *c*-Si-C-N.

ACKNOWLEDGMENTS

One of the authors (W. F. P.) acknowledges support by the National Science Council of the R.O.C., under contract NSC89-2112-M-032-008. This work was performed on the HSGM and DCM beamlines at SRRC.

[1] M. Dayan, J. Vac. Sci. Technol. A **3**, 361 (1985); E. C. Paloura, J. Lagowski, and H. C. Gatos, J. Appl. Phys. **69**, 3995 (1991).

[2] M. L. Cohen, Phys. Rev. B **32**, 7988 (1985); A. Y. Liu and M. L. Cohen, Science **245**, 841 (1989).

[3] A. Gheorghiu, C. Sénémaud, H. Roulet, G. Dufour, T. Moreno, S. Bodeur, C. Reynaud, M. Cauchetier, and M. Luce, J. Appl. Phys. **71**, 4118 (1992).

[4] F. Ténégal, A. M. Flank, and N. Herlin, Phys. Rev. B **54**, 12029 (1996).

[5] L. C. Chen, C. Y. Yang, D. M. Bhusari, K. H. Chen, M. C. Lin, J. C. Lin, T. J. Chuang, Diamond Rel. Mater. **5**, 514 (1996).

[6] J. F. Morar, F. J. Himpsel, G. Hollinger, G. Hughes, and J. L. Jordan, Phys. Rev. Lett. **54**, 1960 (1985).

[7] J. Nithianandam, J. C. Rife, and H. Windischmann, Appl. Phys. Lett. **60**, 135 (1992).

[8] J. Robertson, Phil. Mag. B **66**, 615 (1992).

[9] M.-H. Tsai *et al.* (To be published).

[10] J. Robertson, Phil. Mag. B **63**, 47 (1991).

[11] W. F. Pong *et al.* (To be published).

Figure Captions

Fig. 1 Normalized C *K*-edge absorption spectra of β-SiC, *c*-Si-C-N, and Diamond/Si.

Fig. 2 Normalized N *K*-edge absorption spectra of *c*-Si-C-N and α-Si_3N_4.

Fig. 3 Normalized Si *K*-edge absorption spectra of *c*-Si(100), *c*-Si-C-N, α-Si_3N_4, and β-SiC.

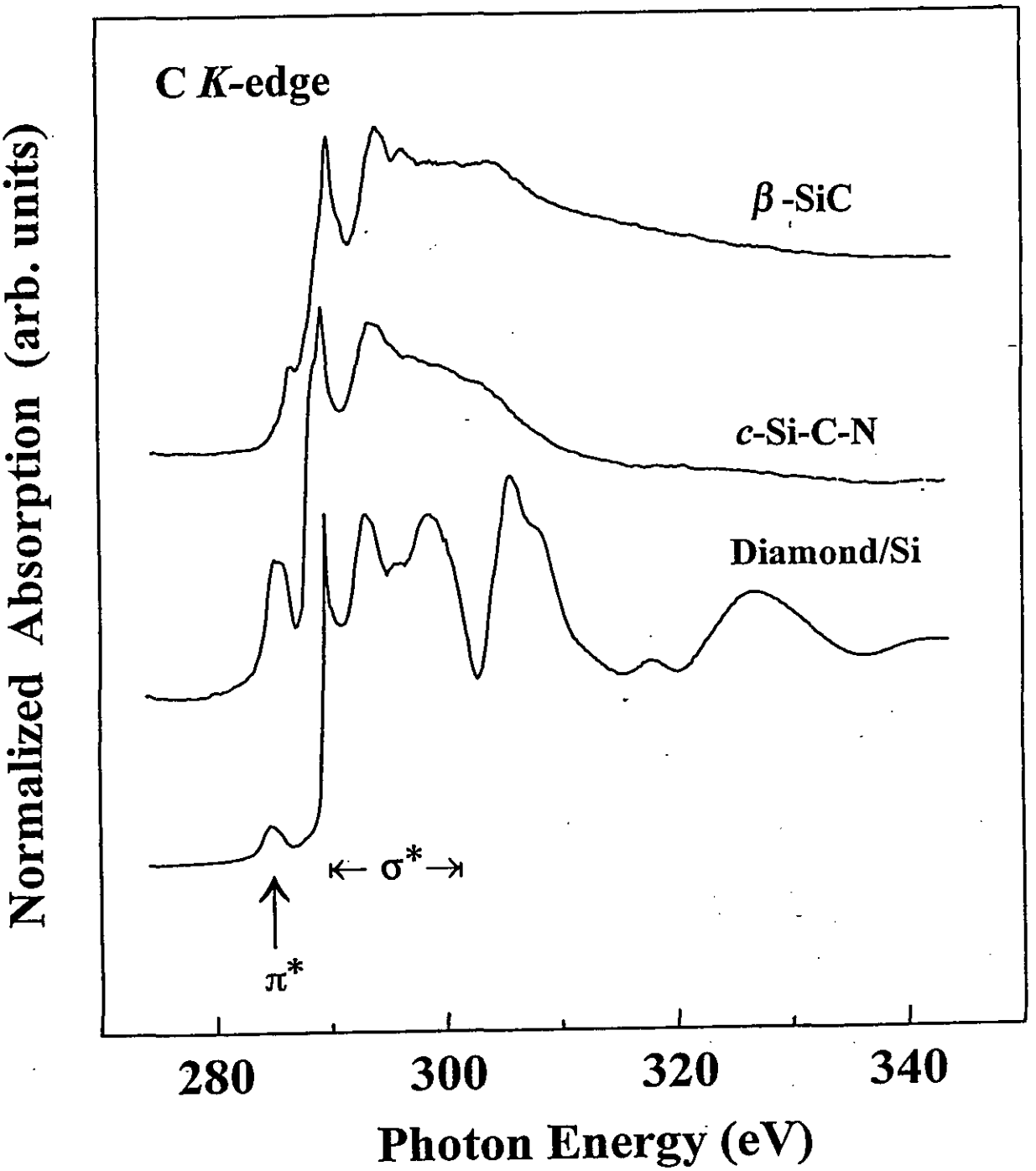
C K-edge
β-SiC
c-Si-C-N
Diamond/Si
← σ* →
π*
Normalized Absorption (arb. units)
280
300
320
340
Photon Energy (eV)

Fig. 1

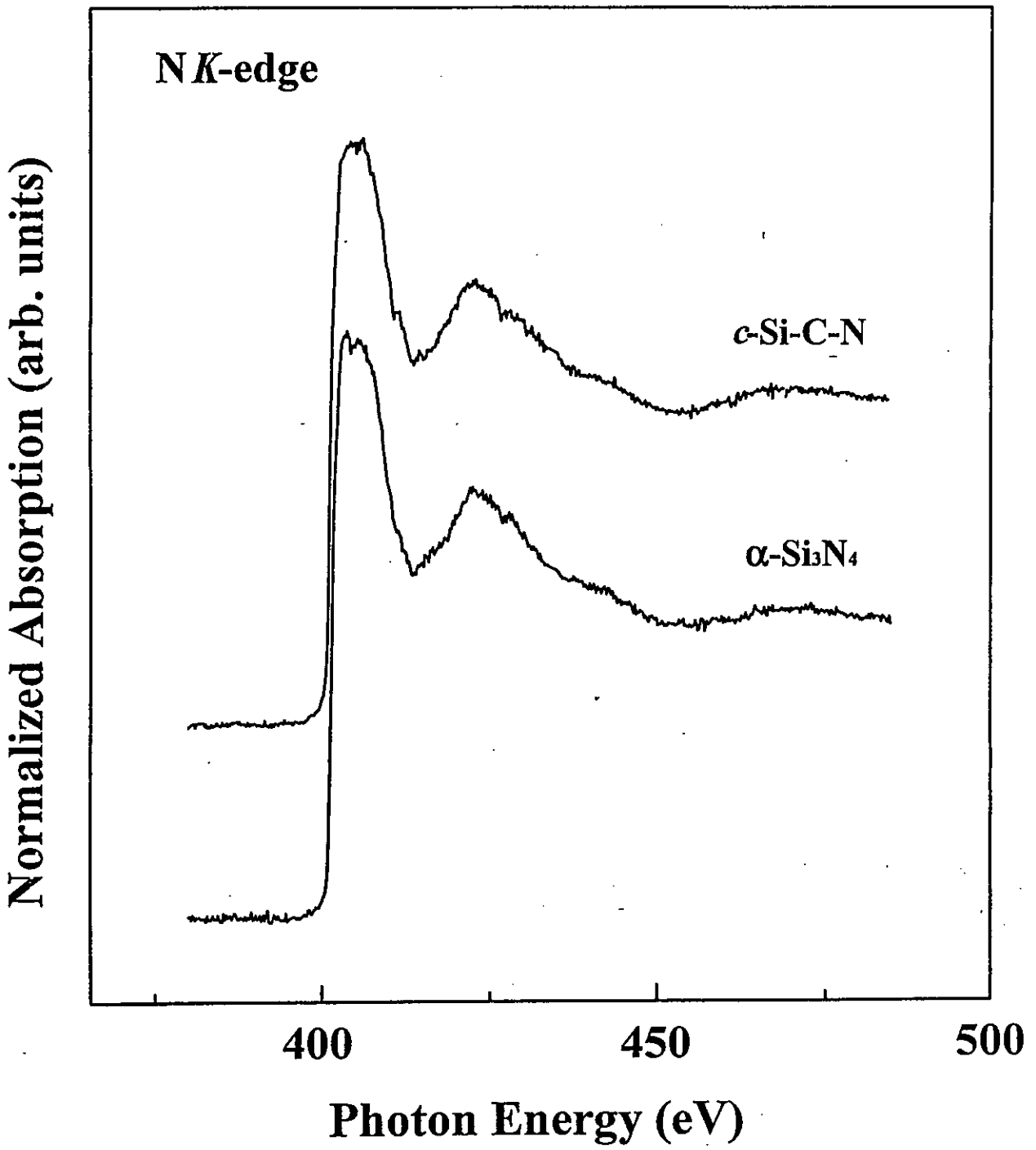
N K-edge
c-Si-C-N
α-Si3N4
Normalized Absorption (arb. units)
400
450
500
Photon Energy (eV)

Fig. 2

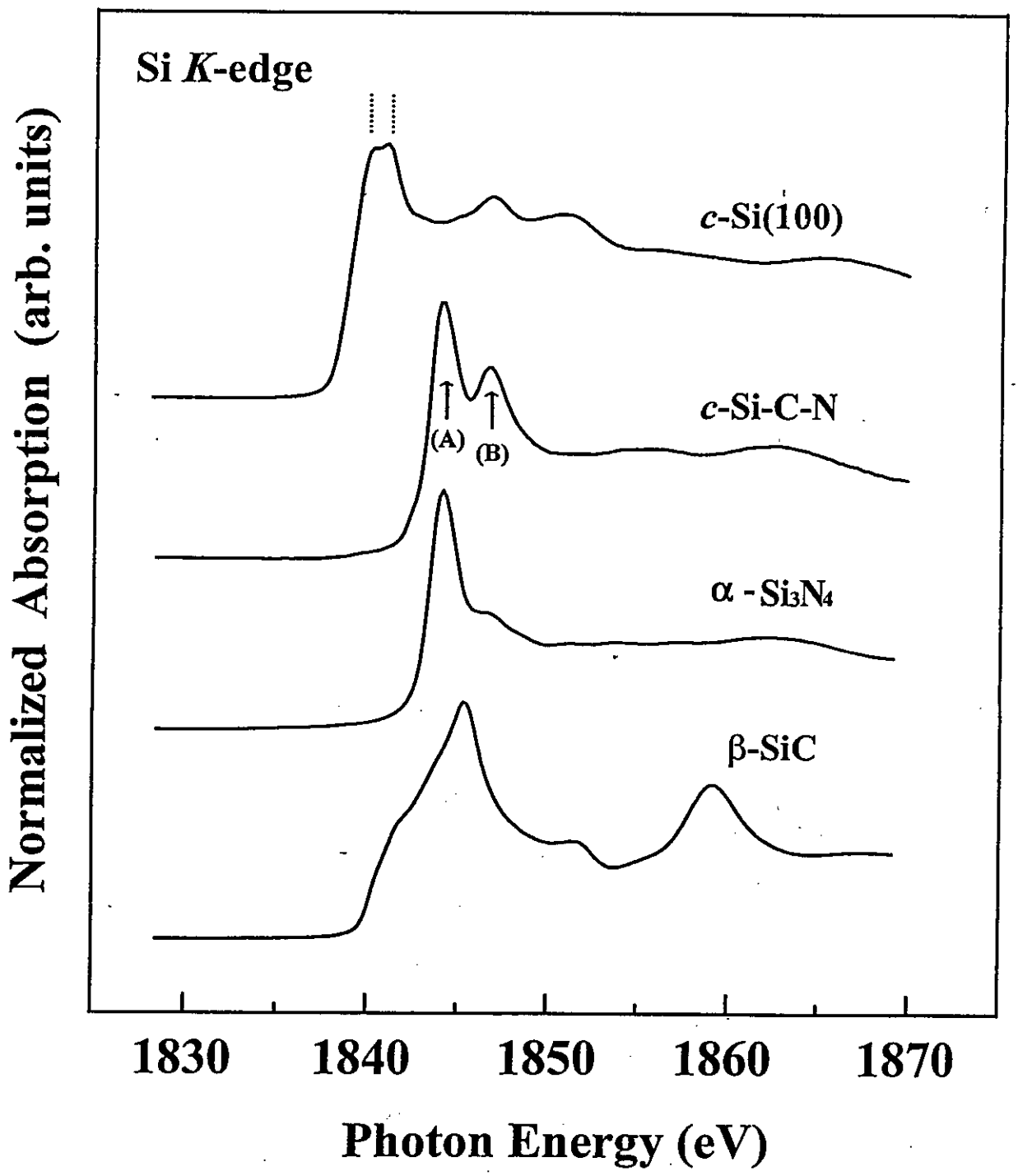
Si K-edge
c-Si(100)
c-Si-C-N
(A)
(B)
α - Si3N4
β-SiC
Normalized Absorption (arb. units)
1830
1840
1850
1860
1870
Photon Energy (eV)

Fig. 3